Design, synthesis and biological evaluation of 4′-aminochalcone-rivastigmine hybrids as multifunctional agents for the treatment of Alzheimer's disease

Ganyuan Xiao, Yan Li, Xiaoming Qiang, Rui Xu, Yunxiaozhu Zheng, Zhongcheng Cao, Li Luo, Xia Yang, Zhipei Sang, Fu Su, Yong Deng

PII: S0968-0896(16)31071-9
DOI: http://dx.doi.org/10.1016/j.bmc.2016.12.013
Reference: BMC 13440

To appear in: *Bioorganic & Medicinal Chemistry*

Received Date: 27 October 2016
Revised Date: 3 December 2016
Accepted Date: 8 December 2016

Please cite this article as: Xiao, G., Li, Y., Qiang, X., Xu, R., Zheng, Y., Cao, Z., Luo, L., Yang, X., Sang, Z., Su, F., Deng, Y., Design, synthesis and biological evaluation of 4′-aminochalcone-rivastigmine hybrids as multifunctional agents for the treatment of Alzheimer's disease, *Bioorganic & Medicinal Chemistry* (2016), doi: http://dx.doi.org/10.1016/j.bmc.2016.12.013

Design, synthesis and biological evaluation of 4′-aminochalcone-rivastigmine hybrids as multifunctional agents for the treatment of Alzheimer's disease

Ganyuan Xiao[a], Yan Li[a], Xiaoming Qiang[a], Rui Xu[a], Yunxiaozhu Zheng[a], Zhongcheng Cao[a], Li Luo[a], Xia Yang[a], Zhipei Sang[b], Fu Su[a,*], Yong Deng[a,*]

[a]*Department of Medicinal Chemistry, Key Laboratory of Drug Targeting and Drug Delivery System of the Education Ministry, West China School of Pharmacy, Sichuan University, Chengdu, 610041, China*

[b]*College of Chemistry and Pharmaceutical Engineering, Nanyang Normal University, Nanyang, 473061, China*

**Corresponding Author*.

Phone, +86-28-85501310; E-mail: sufu@scu.edu.cn (Fu Su)

Phone, +86-28-85503790; E-mail: dengyong@scu.edu.cn (Yong Deng)

Abstract

A series of 4′-aminochalcone-revastigmine hybrids were designed, synthesized and evaluated as multifunctional agents for the treatment of Alzheimer's disease. The results showed that most of these compounds exhibited good multifunctional activities. In particular, compound **6c** displayed the best inhibitory potency on acetylcholinesterase (IC_{50} = 4.91 μM), and significant antioxidative activity with a value 2.83-fold of Trolox. The kinetic analysis of AChE inhibition revealed that **6c** showed mixed-type inhibition, binding simultaneously to the catalytic active site and peripheral anionic site of AChE. In addition, **6c** inhibited self-induced A$\beta_{1\text{-}42}$ aggregation and Cu^{2+}-induced A$\beta_{1\text{-}42}$ aggregation by 89.5% and 79.7% at 25 μM respectively, as well as acted as a selective monoamine oxidase B inhibitor (IC_{50} = 0.29 μM) and a selective biometal chelator. Furthermore, **6c** could cross the blood-brain barrier *in vitro*. Based on these results, Compound **6c** could be considered as a very promising lead compound for Alzheimer's disease.

Keywords:

Alzheimer's disease; Chalcone carbamate derivatives; Multifunctional agents; Acetylcholinesterase inhibitors; Aβ aggregation inhibitors; Monoamine oxidase B inhibitors.

1. Introduction

Alzheimer's disease (AD), featured with dementia, cognitive dysfunction and memory lapse, is one of the most prevalent fatal neurodegenerative disorders among the elderly.[1] Today, 47 million people live with dementia worldwide, and this number is projected to increase to more than 131 million by 2050.[2] Although the etiology of AD is not fully explicated, multiple factors, involving deficits of acetylcholine (ACh), β-amyloid (Aβ) deposits, oxidative stress and dyshomeostasis of biometals, seem to play crucial roles in the progression of the disease.[3] Up to now, acetylcholinesterase inhibitors (AChEIs) are the major and most developed class of drugs approved for AD therapy, such as donepezil, rivastigime, galanthamine and Huperzine A.[4] The cholinergic hypothesis asserts that AChEIs could increase the levels of ACh in AD patients through the inhibition of acetylcholinesterase (AChE), and, therefore, relieve some symptoms of AD patients. However, AChEIs just show modest palliative clinical efficacy without underlying the pathogenic processes or correcting the progressive neurodegeneration.[5]

Among the multiple factors of AD, Aβ plays a central role.[6] The main isoforms of the Aβ peptide are Aβ_{42} and Aβ_{40}. Aβ_{40} is present in larger amounts in the brain, yet Aβ_{42} is more neurotoxic and has a higher tendency to aggregate. A common concept of the amyloid cascade hypothesis is that the aggregation of Aβ_{42} is the main initiating event that sets off the pathogenic cascade, ultimately leading to neuronal loss and dementia.[7] Additionally, excessive biometals such as Cu^{2+}, Fe^{2+}, Zn^{2+} and Al^{3+} have been found within the Aβ deposits in AD brains, and it is well known that interaction of Aβ with redox-active metal ions contributes to the production of reactive oxygen species (ROS).[8] Oxidative stress is one of the earliest events in the progress of AD, and it is shown to affect every class of biological macromolecules, including nucleic acids, proteins, lipids, and carbohydrates. Furthermore, recent studies have indicated that oxidative damage could promote the appearance of amyloid plaques and neurofibrillar tangles in AD.[9] Taken together, successful inhibition of Aβ aggregation, modulation of biometals in the brain and protection of neuronal cells from oxidative stress could potentially prevent AD.

Monoamine oxidase (MAO) is the enzyme that catalyzes the oxidative deamination of various biogenic and xenobiotic amines.[10] Studies have demonstrated that high expression levels of MAO-B in neuronal tissue can increase the level of oxidative free radicals.[11] Therefore, MAO inhibitors can

be acted as potential anti-AD drug candidates due to their capacity to inhibit oxidative stress. Especially, selective MAO-B inhibitors, like selegiline and rasagiline, have been demonstrated to significantly slow the disease progression and improve memory deficits in AD animal models.[12] These observations suggest that selective MAO-B inhibitors may be of value for AD therapy.

Due to the multi-pathogenesis of AD, the development of agents that affect two or more relevant targets has drawn considerable attention for their potential advancements in the treatment of AD. In recent years, many multifunctional agents have been discovered with multiple potencies, including cholinesterase (ChE) inhibition, Aβ deposit inhibition, antioxidative and metal chelating properties.[13-15] Natural products are rich and unexplored sources of novel leading compounds with bioactive properties. One such natural scaffold abundant in edible plants is the chalcone (1,3-diphenyl-2-propen-1-ones), which possesses a broad range of pharmacological activities related to neurological disorders, such as anti-inflammatory, anti-oxidant, neuroprotective properties.[15] Recently, many studies demonstrated that natural chalcone and synthetic analogs exhibited ChE and MAO inhibitory activities, and they are more commonly used as Aβ imaging agents.[16-18] These results indicate that chalcone may be used as a leading compound in the design of multifunctional drugs for the treatment of AD. Moreover, Masahiro Ono *et al*. reported that ^{18}F-labeled chalcone with a dimethylamino group at 4′-position (**Figure 1**, **1**) showed a sufficient brain uptake with a good binding capacity to Aβ plaques (K_i = 39.8 nM).[19] Rivastigmine (**Figure 1**, **2**), a carbamate compound, is approved by the FDA as a ChE inhibitor for the treatment of AD. The carbamate moiety in rivastigmine is the ChE inhibitory pharmacophore, which can covalently bind to the enzyme and remain attached until it is slowly removed by hydrolysis.[20,21] Therefore, we planned to use the multitarget-directed ligand strategy to combine chalcone and rivastigmine, creating a series of chalcone-rivastigmine hybrids (**Figure 1**), in the hope of acquiring novel molecules possessing more potencies in various multifunctional activities.

In this study, a series of chalcone-revastigmine hybrids were designed, synthesized and evaluated for their biological activity, including inhibition of cholinesterase, antioxidant and metal chelating effects, inhibitory effects on Aβ aggregation and MAO and the ability to cross the blood–brain barrier (BBB). The design strategy for chalcone-revastigmine hybrids is depicted in **Figure 1**.

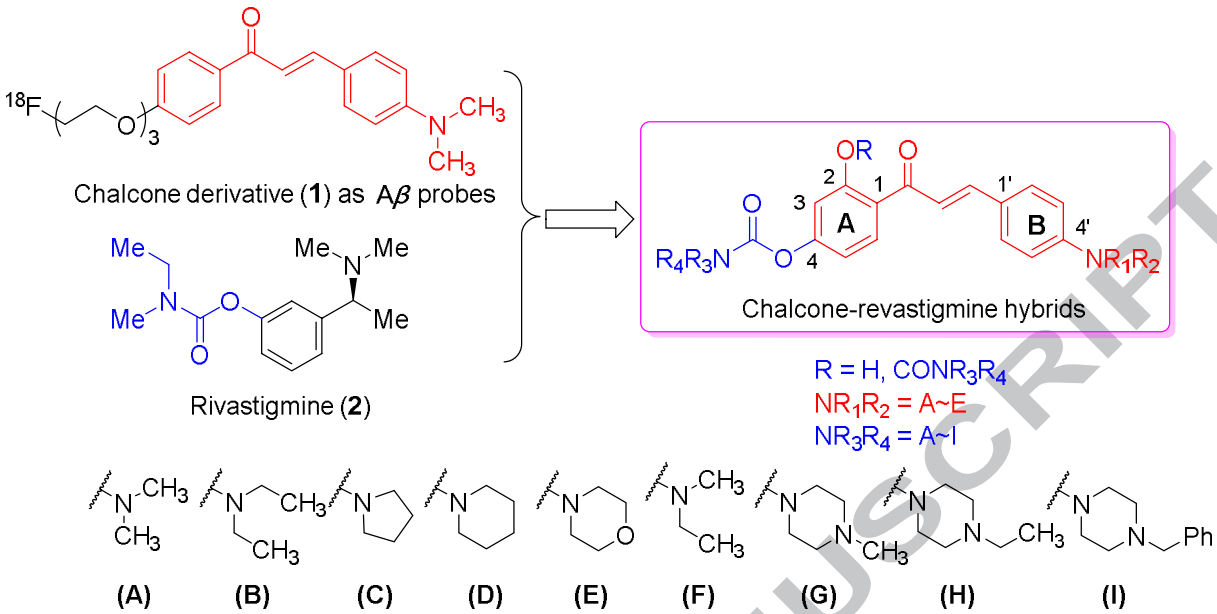

Figure 1. Design strategy for chalcone-revastigmine hybrids

2. Results and discussion

2.1. Chemistry

The synthetic routes for the preparation of 4′-aminochalcone-revastigmine hybrids were depicted in **Scheme 1**. The chalcone scaffolds (**3a-e**) were the key intermediates, derived *via* the aldol condensation of 2,4-dihydroxyacetophenone (**2**) with *p*-aminobenzaldehydes (**1a-e**) in the anhydrous K_2CO_3 and DMF at 100 °C.[22] *N*,*N*-disubstituted carbamoyl chlorides (**5a-i**) were prepared by reaction of corresponding secondary amines (**4a-i**) with triphosgene in the presence of $NaHCO_3$ in anhydrous DCM.[23] Subsequently, *O*-carbamoylation of the compounds **3a-e** was accomplished by the treatment with **5a-i** in the presence of anhydrous K_2CO_3 and a catalytic amount of 4-dimethylaminopyridine (4-DMAP) in CH_3CN at 40-45 °C to afford the desired target compounds (**6a-i**, **7a**, **7c-e**, **8b-e**) in moderate yields. These target compounds have not previously been reported in the literature. Their structures were confirmed by ^{1}H NMR, ^{13}C NMR and ESI-MS.

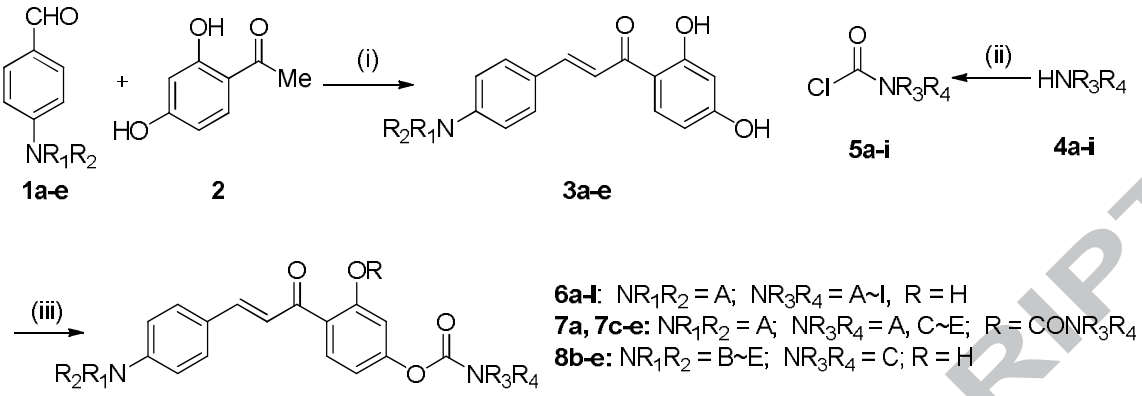

Scheme 1. Synthesis of chalcone-revastigmine hybrids **6-8**. *Reagents and conditions:* (i) K_2CO_3, DMF, 100 °C, 10-12 h; (ii) triphosgene, $NaHCO_3$, CH_2Cl_2, -10~0 °C, 6-8 h; (iii) R_3R_4NCOCl (**5a-i**), 4-DMAP, K_2CO_3,CH_3CN, 40-45 °C, 5-10 h.

2.2. Pharmacology

2.2.1. AChE and BuChE Inhibition

The inhibitory activities of target compounds against AChE (from *electric eel*) and butyrylcholinesterase (BuChE) (from *rat serum*) were measured according to the spectrophotometric method of Ellman *et al*.[24] The inhibitory activities of the target compounds were compared with the parent compound **3a** and the commercially available rivastigmine. The IC_{50} values for AChE and BuChE inhibition were summarized in **Table 1**. These results revealed that the introduction of carbamates increased the AChE inhibitory capacity, which was consistent with our design strategy. Most of the target compounds displayed moderate AChE inhibitory activities with IC_{50} values in the micromolar level, and demonstrated scarcely any BuChE inhibitory activities. The scarcity of BuChE inhibitory activities may be a shortcoming, for BuChE plays a role in regulating the ACh level in the process of AD.[25] However, selective inhibition of AChE over BChE may include fewer side effects associated with peripheral inhibition of cholinesterase, as BuChE is mainly localized in the peripheral tissues.[26] Initially, the hybrids were limited to one head group of dimethylamine at 4′-position and different carbamate tail groups at 4-position, to explore structure-activity relationship (SAR). Compounds with cyclic amine groups (**6c-6e**) at 4-position showed better inhibitory activity than those with non-cyclic amine groups (**6a**, **6b**, **6f**). Noticeably, compound **6c** was the most potent inhibitor with the IC_{50} value of 4.91 ± 0.15 μM, being 2-fold more potent than that of rivastigmine

(IC_{50} = 9.94 ± 0.83 μM). Meanwhile, compounds containing piperazine ring (**6g**, **6h**) at 4-position performed comparatively better, while the compound possessing the benzylpiperazine (**6i**) showed relatively reduced AChE inhibitory activity. In addition, we decided to replace the dimethylamine moiety with several aminoalkyl groups at 4′-position, remaining the optimal side chains pyrrolidine carbamate fixed. Unfortunately, all of them (**8b-8e**) showed weaker inhibitory activity than **6c**. Compound **8e**, containing a hydrophilic morpholine ring, showed significant reduced AChE inhibitory activity, which implied that the hydrophobic interactions in this binding region of the enzymes might be required for intensive inhibition. The results suggested electron-withdrawing effects of oxygen atom might reduce the electronic density of the terminal nitrogen, thereby impacting on protonation at physiological pH, which could diminish the cation–π interaction between the terminal nitrogen and the catalytic active site (CAS) of AChE.[27] Furthermore, we found that introduction of carbamates simultaneously into 2- and 4-position of the chalcone structure resulted in weak AChE inhibitors (**7a**, **7c-7e**), which may result from a change in the overall shape of the molecules, thereby making it difficult for them to align correctly in the gorge leading to the active site.

Table 1. AChE and BuChE inhibitory activities, and oxygen radical absorbance capacity (ORAC, Trolox equivalents) of chalcone-revastigmine hybrids and reference compound.

Compd.	NR_1R_2	NR_3R_4	IC_{50} ± SD[a] (μM)		ORAC[d]
			*Ee*AChE[b]	*Rat*BuChE[c]	
3a		—	78.21 ± 2.04	n.a.[e]	2.00 ± 0.03
6a			32.62 ± 1.78	n.a.	2.62 ± 0.05
6b		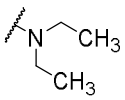	17.21 ± 1.21	n.a.	2.20 ± 0.02
6c			4.91 ± 0.15	n.a.	2.83 ± 0.05
6d			6.90 ± 0.53	n.a.	2.51 ± 0.05
6e	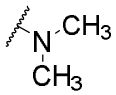		8.01 ± 0.71	n.a.	2.04 ± 0.04

6f	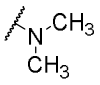		14.33 ± 0.80	n.a.	3.14 ± 0.05
6g	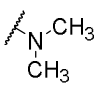	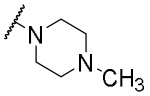	11.94 ± 0.79	n.a.	2.08 ± 0.04
6h	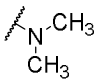	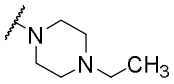	8.62 ± 0.81	n.a.	2.54 ± 0.02
6i	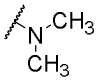	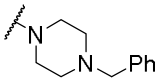	21.43 ± 1.63	n.a.	3.51 ± 0.09
7a	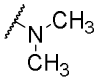		> 100	n.a.	2.16 ± 0.04
7c	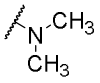		30.02 ± 2.29	n.a.	2.45 ± 0.05
7d	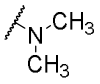		32.44 ± 2.02	n.a.	2.41 ± 0.03
7e	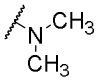		58.01 ± 2.94	n.a.	1.85 ± 0.04
8b	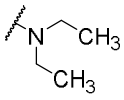		11.74 ± 0.92	n.a.	1.02 ± 0.02
8c			14.06 ± 1.10	n.a.	0.35 ± 0.01
8d			10.62 ± 1.33	n.a.	1.20 ± 0.02
8e			63.50 ± 1.93	n.a.	0.51 ± 0.01
Rivastigmine			9.94 ± 0.83	2.86 ± 0.22	NT[f]

[a] IC_{50} values represent the concentration of inhibitor required to decrease enzyme activity by 50% and are the mean of 3 independent experiments, each performed intriplicate (SD = standard deviation).

[b] AChE from *electric eel* (*Ee*AChE).

[c] BuChE from rat serum and tested compounds were used at 50 μM.

[d] The mean SD of the 3 independent experiments. Data are expressed as μM of Trolox equivalent/μM of tested compound.

[e] n.a. = no active. Compounds defined "no active" means a percent inhibition of less than 10.0% at a concentration of 50 μM in the assay conditions.

[f] NT = not tested.

2.2.2. Kinetic characterization of AChE inhibition

To gain further insight into the mechanism for this class of derivatives on AChE, a kinetics study was carried out with compound **6c** using *E*eAChE.[28,29] Graphical analysis of the reciprocal

Lineweaver-Burk plots (**Figure 2**) showed both increasing slopes (decreased V_{max}) and intercepts (higher K_m) at increasing concentration of the inhibitor. The intersection point of the Lineweaver−Burk reciprocal plot fell in the second quadrant, which was indicative of mixed-type inhibition. The result revealed that compound **6c** was able to simultaneously bind to both CAS and peripheral anionic site (PAS) of AChE.

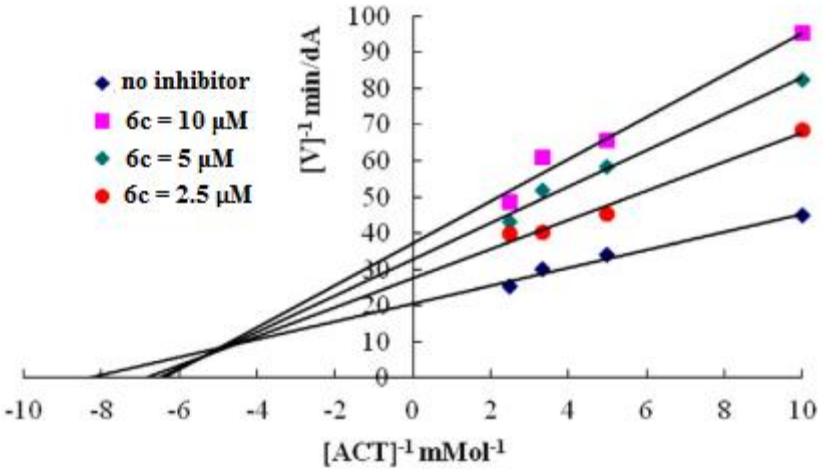

Figure 2. Kinetic study on the mechanism of *Ee*AChE inhibition by **6c**. Overlaid Lineweaver–Burk reciprocal plots of AChE initial velocity at increasing substrate concentrations (0.1–0.4 mM) in the absence of inhibitor and in the presence of **6c** are shown. Lines were derived from a weighted least-squares analysis of data points.

2.2.3. Antioxidant activity

The antioxidant activities of the target compounds were measured by the oxygen radical absorbance capacity assay using fluorescein (ORAC-FL).[30] Trolox, a water-soluble vitamin E analog, was used as a reference standard. The activities of tested compounds to scavenge radicals were expressed as Trolox equivalent, and their relative activities at concentration of 5 μM were compared with the highly potent compound Trolox. As shown in **Table 1**, all the compounds displayed moderate to excellent antioxidant activity with ORAC-FL values in the range of 0.51–3.51 Trolox equivalents. In particular, compounds **6c**, **6f** and **6i** exhibited the most potent antioxidant activities with ORAC-FL values of 2.83 ± 0.05, 3.14 ± 0.05 and 3.51 ± 0.09 Trolox equivalents respectively. Generally, the 2- and 4-disubstituted homologues (**7a**, **7c-7e**) were a little weaker than the corresponding 2-unsubstituted homologues (**6a**, **6c-6e**) in terms of antioxidant activity, which was consistent with our previous research.[31] The 2-OH of derivatives, which can form intramolecular

hydrogen, was beneficial to improve the radical scavenging ability to some degree.[32,33] Furthermore, all the 4′-dimethylamine chalcone-rivastigmine hybrids **(6a-6i)** showed decent antioxidant activity and replacement of the 4′-dimethylamine with other aminoalkyl groups (**8b-8e**) presented a considerable loss of antioxidant activity. From these results, it may be concluded that dimethylamine substitution at 4′-position of chalcone is favorable for antioxidant potency.

2.2.4. Metal-chelating properties

Study revealed that the fragment of 2-hydroxy and ketone group in chalcone, which can form intramolecular hydrogen, is responsible for the metal-chelating properties.[34] To investigate the metal-chelating properties of the series of hybrids, we selected **6c** as a typical example. The metal-chelating ability of **6c** was investigated using UV-vis spectrometry.[35] The results were shown in **Figure 3A**. After $CuCl_2$ was added to a solution of **6c**, the maximum absorption wavelength shifted from 441 nm to 482 nm, indicating the formation of **6c**-Cu^{2+} complexes. Similar result was obtained when $AlCl_3$ was added: the peak in the electronic spectra of **6c** at 441 nm shifted to 522 nm. However, there was little change on the UV spectrum after adding $FeSO_4$ and $ZnCl_2$. Therefore, **6c** displayed selective metal chelation. The stoichiometry of the **6c**-Cu^{2+} complex was determined using the molar ratio method by preparing solutions of compound **6c** with increasing amounts of $CuCl_2$. The UV spectra was used to obtain the absorbance of the complex of **6c** and $CuCl_2$ at different concentrations at 474 nm. As shown in Figure **3B**, the absorbance initially increased linearly and then became stable. The two straight lines intersected at a mole fraction of 0.98, revealing a 1:1 stoichiometry for the complex.

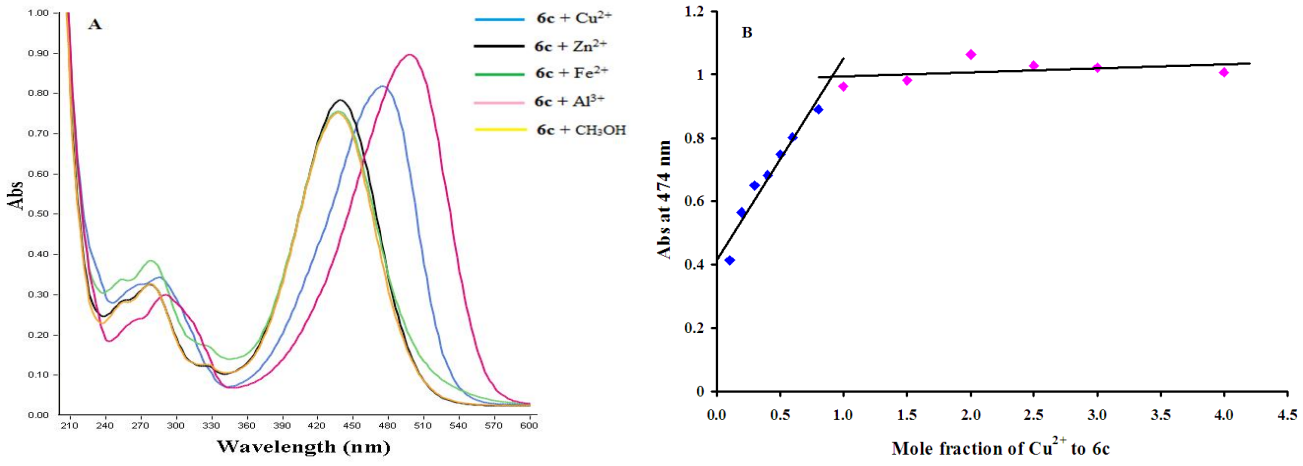

Figure 3. A) UV spectra of compound **6c** (37.5 μM in methanol) alone or in the presence of $CuCl_2$, $ZnCl_2$, $FeSO_4$ or $AlCl_3$ (37.5 μM, in methanol). **B)** Determination of the stoichiometry of

complex-Cu^{2+} by using the molar ratio method of titrating the methanol solution of compound **6c** with ascending amounts of $CuCl_2$. The final concentration of tested compound was 37.5 μM, and the final concentration of Cu^{2+} ranged from 3.75 to 150 μM.

2.2.5. Effects on the Aβ aggregation

To investigate the activity of our synthetic compounds to inhibit the self- and Cu^{2+}-induced Aβ_{1-42} aggregation, the Thioflavin T (ThT) fluorescence assay was performed, with curcumin as the reference compound.[27,35,36] As shown in **Table 2**, 4-dimethylamino chalcone scaffold (**3a**) exhibited a significant ability to inhibit Aβ_{1-42} aggregation and the introduction of various carbamate fragments could further raise the value of inhibition ratio. These derivatives showed moderate to decent inhibitory potencies of self- and Cu^{2+}-induced Aβ_{1-42} aggregation (33.3-98.0% and 23.8-89.4% at 25 μM, respectively), compared with that of curcumin (41.3 ± 0.9% and 67.2 ± 1.3% at 25 μM, respectively). The compounds with the most potent inhibition effects on self-induced Aβ_{1-42} aggregation were **6a**, **6f**, **6i**, with respective inhibition ratio of 90.8 ± 1.8%, 98.0 ± 1.9% and 89.4 ± 1.4%, while the optimal Cu^{2+}-induced Aβ_{1-42} aggregation inhibition properties were provided by **6f** (88.0 ± 2.4%), **6h** (89.2 ± 1.9%) and **6i** (94.2 ± 1.6%), respectively. Unlike the trend of AChE inhibition, the different kinds of carbamate moieties had little effects on the Aβ_{1-42} aggregation inhibitory activity, for the inhibition ratio of **6a-6i** showed unconspicuous diversities. Noticeably, the potencies of 4-*O*-modified derivatives (**6a-6i**) were much higher than those of 2, 4-*O*-bis-modified derivatives (**7a**, **7c-7e**). It revealed that exposure of hydroxy group at 2-position, which can form hydrogen bond, is crucial for enhancing inhibition effect. The potencies of **8b-8e** were relatively weaker than that of **6c**, indicating that 4′-dimethylamino group may intensify the interaction between derivatives and Aβ_{1-42} protein.

Table 2 Inhibition of self- and Cu^{2+}-induced Aβ_{1-42} aggregation, recombinant human MAO-A and -B of chalcone-revastigmine hybrids and reference compounds.

Compd.	%Inhibition of Aβ_{1-42} aggregation[a]		IC_{50} ± SD (μM)		SI[e]
	Self-induced[b, f]	Cu^{2+}-induced[c, f]	MAO-A[d, f]	MAO-B[d, f]	
3a	77.7 ± 1.6	60.1 ± 2.1	4.06 ± 0.084	0.31 ± 0.031	13.36
6a	90.8 ± 1.8	77.9 ± 1.9	10.20 ± 0.094	2.48 ± 0.045	4.11
6b	76.7 ± 2.0	49.0 ± 1.1	24.4 ± 1.4%	3.50 ± 0.103	>0.87
6c	89.5 ± 1.2	79.7 ± 1.9	12.8 ± 1.1%	0.29 ± 0.021	>34.97

6d	70.2 ± 1.1	73.9 ± 1.7	27.8 ± 1.6%	31.1% ± 1.4%	—
6e	83.6 ± 1.4	79.7 ± 1.3	34.6 ± 2.1%	42.3% ± 1.8%	—
6f	98.0 ± 1.9	88.0 ± 2.4	25.9 ± 2.0%	2.10 ± 0.041	>4.76
6g	87.9 ± 1.8	75.5 ± 2.3	49.5 ± 2.1%	25.1% ± 1.2%	—
6h	83.2 ± 1.2	89.2 ± 1.9	42.5 ± 2.2%	30.0% ± 2.1%	—
6i	89.4 ± 1.4	94.2 ± 1.6	42.1 ± 2.1%	41.6% ± 2.7%	—
7a	34.7 ± 1.5	56.2 ± 1.1	34.6 ± 1.9%	5.1% ± 1.1%	—
7c	48.0 ± 0.8	26.3 ± 0.8	25.2 ± 1.0%	34.6% ± 2.1%	—
7d	38.0 ± 0.7	23.8 ± 0.6	17.0 ± 0.9%	30.1% ± 1.9%	—
7e	33.3 ± 1.2	41.4 ± 1.1	15.0 ± 0.6%	40.2% ± 1.7%	—
8b	67.8 ± 1.0	67.1 ± 1.2	21.0 ± 1.1%	6.70 ± 0.201	>0.59
8c	44.4 ± 1.8	48.9 ± 1.7	15.2 ± 1.3%	0.71 ± 0.024	>14.07
8d	57.2 ± 1.9	59.8 ± 2.1	19.6 ± 1.2%	0.78 ± 0.032	>12.82
8e	44.4 ± 0.8	48.9 ± 1.7	15.2 ± 1.1%	0.71 ± 0.033	>14.07
Curcumin	41.3 ± 0.9	67.2 ± 1.3	—	—	—
Clorgyline	—	—	0.0027 ± 0.0006	4.19 ± 0.101	0.00064
Rasagiline	—	—	1.42 ± 0.015	0.083 ± 0.002	17.21
Iproniazid	—	—	2.56 ± 0.023	1.95 ± 0.074	1.31

[a] For inhibition of Aβ aggregation, the thioflavin-T fluorescence method was used.

[b] Inhibition of self-induced A$\beta_{1\text{-}42}$ aggregation (25 μM) by tested inhibitors at 25 μM.

[c] Inhibition of Cu^{2+}-induced A$\beta_{1\text{-}42}$ aggregation. The concentration of tested compounds and Cu^{2+} were 25 μM.

[d] Percentages are the percent inhibition of MAO by tested compounds at 10 μM.

[e] SI = IC_{50} (MAO-A) / IC_{50} (MAO-B)

[f] The mean ± SD of the three independent experiments.

2.2.6. Recombinant human MAO-A and -B inhibition studies

To complete the study of the multi-target biological profile of the hybrid compounds, the inhibitory activities against recombinant human MAO-A and -B were determined, with the established MAOIs, clorgyline, rasagiline, and iproniazid, applied for comparative purposes.[37-39] It could be seen from the **Table 2** that the parent compound **3a** exhibited potent MAO-A and -B inhibitory activity (IC_{50} = 4.06 ± 0.084 μM for MAO-A; IC_{50} = 0.31 ± 0.031 μM for MAO-B), and the introduction of various carbamate moieties resulted in a dramatic drop of MAO-A inhibition. It was apparent that most of the 4-*O*-modified hybrids could effectively inhibit MAO-B with IC_{50} ranging from micromolar to sub-micromolar, while no compound showed significantly inhibitory activity for MAO-A, indicating that most of the hybrids are clearly selective MAO-B inhibitors. Compounds **6a**, **6b**, **6f**, bearing carbamates of non-cyclic amine groups at 4-O position, inhibited MAO-B relatively potently and also showed moderate selectivity for MAO-B. Compounds

containing cyclic amine groups (**6d**, **6e**, **6g-6i**), demonstrated quite lower MAO-B inhibition activities, with the exception of **6c**, which was found to be the most potent MAO-B inhibitor (IC_{50} = 0.29 ± 0.021 μM). Compound **6c** was also endowed with the highest selectivity towards MAO-B of all, being more than 26.7 times and 2.0 times higher than that of Iproniazid and Rasagiline respectively. Transforming dimethylamino at 4′-position to other aminoalkyl groups to yield **8b**-**8e** could lead to a slight loss of MAO-B inhibition potency compared with **6c**, in line with the above outcome of A$\beta_{1\text{-}42}$ aggregation assays. The low potency of **7a, 7c-e** suggested that carbamate group at 2-position was unprofitable.

2.2.7. Molecular docking study

To explore a possible interacting mode of the chalcone carbamate derivatives with *Tc*AChE (PDB code: 1EVE), a molecular modeling study was performed using the docking program, AutoDock 4.2 package.[9] The result was shown in **Figure 4**. The docking study showed that compound **6c** occupied the entire enzymatic CAS, the mid-gorge sites and the PAS, and could bind simultaneously to both the catalytic and peripheral site. In the *Tc*AChE-**6c** complex, the B ring of the chalcone moiety in **6c** bond to the PAS via the π-π interactions with Phe288, Phe331 and Phe290, and also engaged in hydrophobic interactions with residues Ile287, Arg289, Leu282. In addition, the α, β-unsaturated ketone in **6c** folded in a conformation in the gorge that allowed it to interact with Tyr334 via the hydrophobic interaction. The A ring of chalcone moiety could bind to the middle gorge by establishing a π-π stacking interaction with the Phe330, and the 2-hydroxy at the chalcone nucleus could bind to the Tyr121 via the intermolecular hydrogen bond. The substituted carbamate fragment of **6c** was observed to bind to the CAS via potential hydrophobic interactions with residues Acn85, Asp72 and Gln69. The simultaneous binding of **6c** with CAS, PAS and the active gorge of *Tc*AChE provides an explanation for its highly potent inhibitory activity for AChE and thus revealed a mixed-type inhibition for this compound.

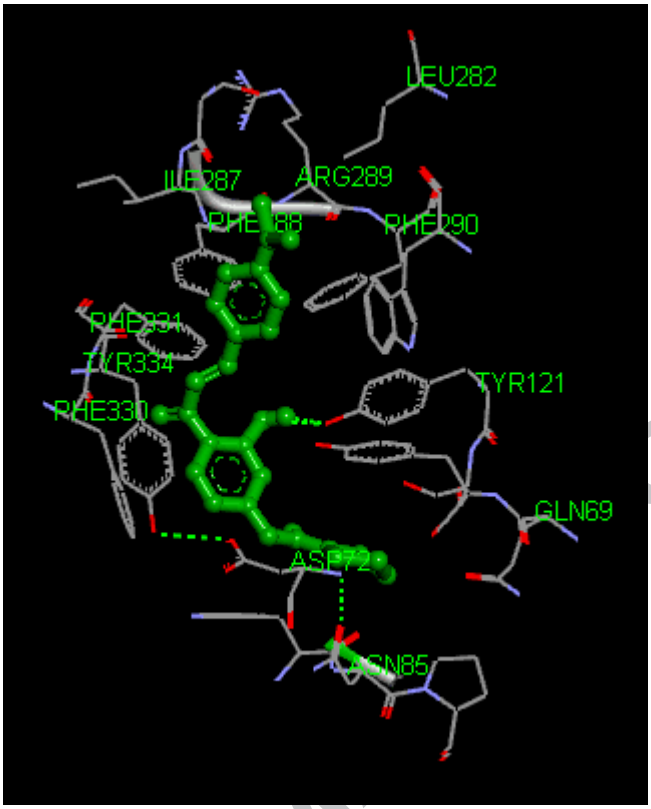

Figure 4. Hypothetical binding mode of compound **6c** interacting with residues in the binding site of *Tc*AChE (1EVE). The protein residues that participate in the main interactions with the inhibitor are labeled.

Furthermore, in order to evaluate the binding modes of this class of chalcone derivatives with respect to human MAO-B, docking simulation was carried out using the docking program, AutoDock 4.2 package based on the X-ray crystal structures of human MAO-B (PDB code: 2V60).[35] On the basis of the in vitro inhibition results, we selected compound **6c**, the most potent MAO-B inhibitor, as a typical ligand for the evaluation. As shown in Figures **5** and **6**, the dimethylamine group of chalcone moiety was properly oriented to the flavin adenine dinucleotide (FAD) cofactor, adopting parallel π-π interactions with Tyr398 and Tyr435. Furthermore, the B-ring of **6c** adopted parallel π-π interactions with Tyr326. The hydroxyl group at 2-position and carbonyl group at 1-position interacted with Ile199 and Phe168 via two hydrogen bonds (Ile199=O • • • HO-**6c**; Phe168-OH • • • O=**6c**). Besides, the carbamate group embedded into a hydrophobic pocket delimited by many hydrophilic acids, such as Pro102, Leu88, Thr312, Thr201, Ile199, Tyr326.

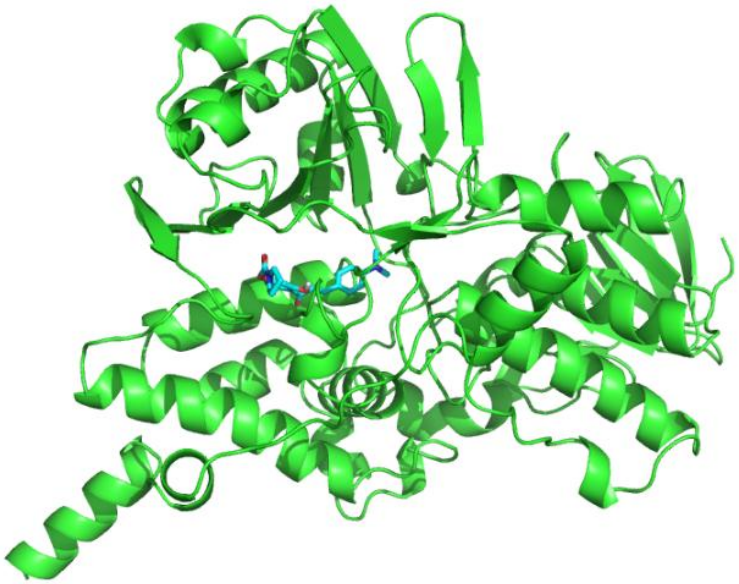

Figure 5. Predicted positions of **6c** into hMAO-B catalytic sites. Compound **6c** and the FAD cofactor were depicted using stick and space fill, respectively.

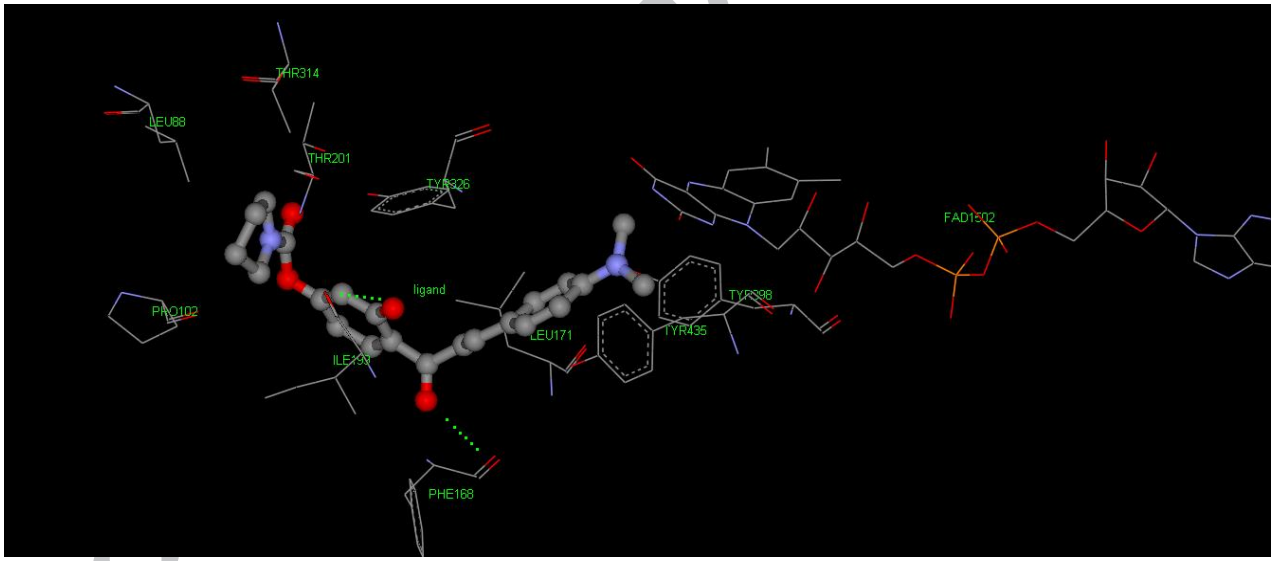

Figure 6. Representation of compound **6c** docked into the binding site of hMAO-B, highlighting the protein residues that form the main interactions with the inhibitor. Hydrogen-bonding interactions between ligand and residues are shown with the green line.

2.2.8. *In vitro* blood-brain barrier permeation assay

Brain penetration is a major requirement for successful central nervous system (CNS) drugs. To evaluate the brain penetration of **6c**, we used a parallel artificial membrane permeation assay for the blood-brain barrier (PAMPA-BBB), as recently described by Di *et al.*[35,40,41] We compared the

permeability of 11 commercial drugs with reported values to validate the assay (**Table 3**). A plot of the experimental data versus the reported values produced a good linear correlation, P_e (exp.) = 0.8792 × P_e (bibl.) − 0.0616 (R^2 = 0.9555) (**Figure 7**). From this equation and considering the limit established by Di *et al.* for blood−brain barrier permeation, we determined that compounds with permeabilities above 3.46 × 10^{-6} cm/s could cross the blood−brain barrier (**Table 4**).[41] Then, the selected compound **6c** was then tested in the PAMPA-BBB assay. The results presented in **Table 5** showed that **6c** could penetrate into the CNS and reach their biological targets located in the CNS.

Table 3. Permeability P_e (× 10^{-6} cm/s) in the PAMPA-BBB assay for 11 commercial drugs used in the experiment validation.

Commercial drugs	Bibl[a]	PBS/EtOH (70:30)[b]
Verapamil	16	16.20 ± 0.20
Oxazepam	10	9.20 ± 0.16
Diazepam	16	10.90 ± 0.32
Clonidine	5.3	5.50 ± 0.18
Imipramine	13	11.20 ± 0.29
Testosterone	17	15.50 ± 0.30
Caffeine	1.3	1.22 ± 0.04
Enoxacine	0.9	0.55 ± 0.03
Piroxicam	2.5	0.84 ± 0.02
Norfloxacin	0.1	0.33 ± 0.01
Theophylline	0.12	0.17 ± 0.005

[a] Taken from Ref.[37]

[b] Data are the mean ± SD of three independent experiments.

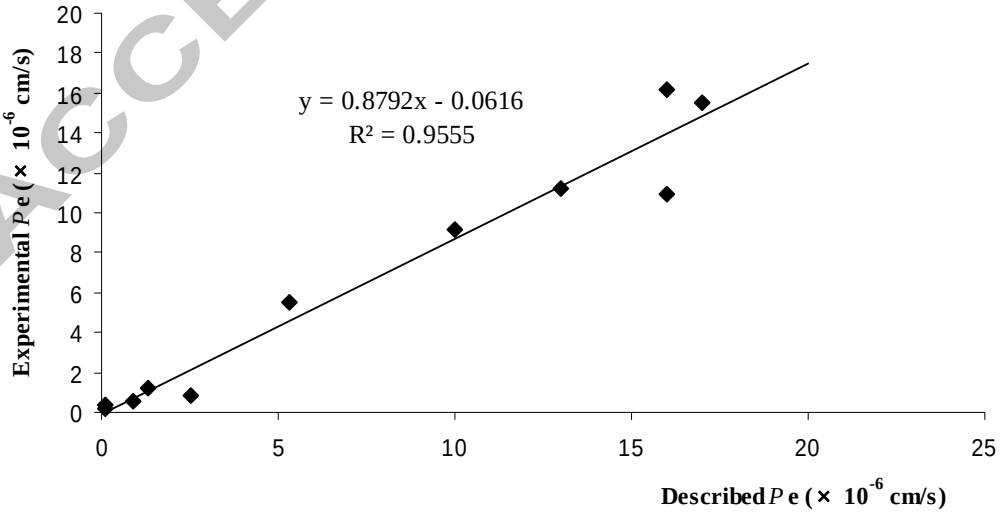

Figure 7. Lineal correlation between experimental and reported permeability of commercial drugs using the PAMPA-BBB assay. P_e (exp) = 0.8792 × P_e (bibl.) − 0.0616 (R^2 = 0.9555).

Table 4. Ranges of permeability of PAMPA-BBB assays ($P_e \times 10^{-6}$ cm/s)

High BBB permeation predicted (CNS +)	$P_e > 3.46$
Uncertain BBB permeation (CNS +/-)	$3.46 > P_e > 1.70$
Low BBB permeation predicted (CNS -)	$P_e < 1.70$

Table 5. Permeability results P_e ($\times 10^{-6}$ cm/s) from the PAMPA-BBB assay for selected aurone derivatives with their predicted penetration into the CNS.

Compd.[a]	P_e ($\times 10^{-6}$ cm/s)[b]	Prediction
6c	7.03 ± 0.19	CNS +

[a] Compound **6c** were dissolved in DMSO at 5 mg/mL and diluted with PBS/EtOH (70:30). The final concentration of each compound was 100 μg/mL.

[b] Data are the mean ± SD of three independent experiments.

3. Conclusion

In conclusion, a series of 4′-aminochalcone-rivastigmine hybrids were designed, synthesized and evaluated as multifunctional agents for the treatment of AD. Most of the synthesized compounds showed potent AChE inhibitory activity and decent inhibitory activities of self- and Cu^{2+}-induced Aβ_{1-42} aggregation *in vitro*. Compound **6c** demonstrated the best inhibitory activity toward AChE with IC_{50} value of 4.91 ± 0.15 μM. The inhibition kinetic analysis suggested that compound **6c** showed a mixed-type inhibition, binding to both CAS and PAS of AChE. Compound **6c** also possessed excellent antioxidant activity (2.83 ± 0.05 Trolox equivalents), excellent inhibitory effects on self-induced Aβ_{1-42} aggregation (89.5 ± 1.2%) and Cu^{2+}-induced Aβ_{1-42} aggregation (79.7 ± 1.9%). With regard to inhibition of MAO, most of target components displayed selective MAO-B inhibitory activity, among which **6c** presented decent IC_{50} values of 0.29 ± 0.021 μM towards MAO-B inhibition. Moreover, **6c** also possessed the prospective property of acting as a metal chelator and permeating BBB. These properties highlighted that the compound **6c** could be considered as a very promising lead compound for Alzheimer's disease.

4. Experimental section

4.1. Chemistry

Melting points were gauged on YRT-3 melting-point apparatus (China) without correction. ^{1}H NMR and ^{13}C NMR spectra were recorded at room temperature in $CDCl_3$ solutions with a Varian INOVA spectrometer. Chemical shifts were expressed in parts per millions (ppm) relative to tetramethylsilane (TMS). Mass spectra were recorded on Agilent-6210 TOF LC-MS Spectrometer. The purity of all final compounds was determined by high-performance liquid chromatography (HPLC) analysis to be over 97%. HPLC analysis was carried out on a Shimadzu LC-10Avp plus system with the use of a Diamonsil C_{18} column (4.6 mm × 150 mm, 5 μM), the compounds eluted with acetonitrile/water/glacial acetic acid, 40:60:1, at a flow rate of 1.0 mL/min). All reagents, unless otherwise specified, were used as high grade commercial products and solvents were of analytical grade. Reaction progress was monitored by thin-layer chromatography (TLC) on silica gel GF254 plates from Qingdao Haiyang Chemical Co. Ltd. (China), and then visualized in an iodine chamber or with an UV lamp (254 nm). Crude products were purified by column chromatography using silica gel (230-400 mesh) from Qingdao Haiyang Chemical Co. Ltd. (China).

4.1.1. General procedure for the synthesis of chalcones (3a-e)

Substituted benzaldehyde **1a-e** (15 mol) was added portionwise to a solution of 2,4-dihydroxy acetophenone **2** (1.5 g, 10 mol) and anhydrous K_2CO_3 (2.76 g, 20 mol) in DMF (15 mL), and the mixture was refluxed for 10-12 h, cooled to room temperature, diluted with EtOAc, and basified with 10% NaOH to pH 9.0. The aqueous phase was separated and neutralized with glacial acetic acid to pH 5.0. The precipitated solid was filtered, washed with cold water, dried in vacuum to give compounds **3a-e** as yellow solids, which were used without further purification.

4.1.2. General procedure for the synthesis of *N,N*-disubstituted carbamoyl chlorides (5a-i)

Compounds **5a-i** were prepared as previously described.[23]

4.1.3. General procedure for the synthesis of 4′-amino chalcone-revastigmine hybrids (6a-i, 7a, 7c-e and 8b-e)

N,N-Disubstituted carbamoyl chlorides **5a-i** (1.59 mmol) was added dropwise to a mixture of anhydrous K_2CO_3 (124.52 mg, 0.90 mmol), 4-DMAP (5.0 mg, 0.039 mmol) and the appropriate intermediates **3a-e** (0.53 mmol) in 2 ml MeCN. The reaction mixture was warmed to 40-45 °C and stirred for 5–10 h under an argon atmosphere to yield carbamylchalcone and 2,4-biscarbamyl chalcone simultaneously. After the reaction was completed, the mixture was concentrated, diluted

with water (20 mL), and extracted with CH_2Cl_2 (20 mL × 3). The combined organic phases were washed sequentially with saturated aqueous Na_2CO_3 (5 mL × 3), saturated aqueous NaCl (10 mL), dried over anhydrous Na_2SO_4, and evaporated to dryness under reduced pressure. The crude product was separated and purified by silica gel flash column chromatography using mixtures of petroleum ether/acetone as eluent to obtain corresponding target compounds **6a-i**, **7a**, **7c-e**, and **8b-e**. The solid of carbamylchalcone (**6a-i**, **8b-e**) was further recrystallized with EtOH and dried *in vacuo* to guarantee crystals of sufficient purity.

4.1.3.1. (*E*)-4-(3-(4-(dimethylamino)phenyl)acryloyl)-3-hydroxyphenyl dimethylcarbamate (6a)

Compound **3a** and **5a** were processed as above to afford product **6a**. Elution with petroleum ether/acetone = 3:1 and further recrystallization with EtOH gave **6a** as a yellow solid, 98.2% HPLC purity, mp 201.2-203.5 °C, yield 45.2%. ^{1}H NMR (600 MHz, $CDCl_3$) δ 13.43 (s, 1H), 7.91 (d, J = 9.6 Hz, 1H), 7.90 (d, J = 13.8 Hz, 1H), 7.57 (d, J = 8.4 Hz, 2H), 7.39 (d, J = 13.8 Hz, 1H), 6.76 (s, 1H), 6.75 (d, J = 9.6 Hz, 1H), 6.70 (d, J = 8.4 Hz, 2H), 3.10 (s, 3H), 3.06 (s, 6H), 3.03 (s, 3H). MS m/z: 355.2 $[M+H]^+$.

4.1.3.2. (*E*)-4-(3-(4-(dimethylamino)phenyl)acryloyl)-1,3-phenylene bis(dimethylcarbamate) (7a)

Compound **3a** and **5a** were processed as above to afford product **7a**. Elution with petroleum ether/acetone = 3:1 gave **7a** as a yellow solid, 99.2% HPLC purity, mp 79.1-80.2 °C, yield 40.3%. ^{1}H NMR (400MHz, $CDCl_3$) δ 7.63 (d, J = 9.2 Hz, 1H), 7.53 (d, J = 15.6 Hz, 1H), 7.45 (d, J = 8.8 Hz, 2H), 7.09 (s, 1H), 7.08 (d, J = 9.2 Hz , 1H), 6.93 (d, J = 15.6 Hz, 1H), 6.66 (d, J = 8.8 Hz, 2H), 3.09 (s, 3H), 3.03 (s, 6H), 3.02 (s, 3H), 2.96 (s, 3H), 2.90 (s, 3H). MS m/z: 426.2 $[M+H]^+$.

4.1.3.3. (*E*)-4-(3-(4-(dimethylamino)phenyl)acryloyl)-3-hydroxyphenyl diethylcarbamate (6b)

Compound **3a** and **5b** were processed as above to afford product **6b**. Elution with petroleum ether/acetone = 2:1 and further recrystallization with EtOH gave **6b** as a yellow solid, 98.0% HPLC purity, mp 145.7-148.0 °C, yield 47.2%. ^{1}H NMR (600 MHz, $CDCl_3$) δ 13.42 (s, 1H), 7.91 (d, J = 15.6 Hz, 1H),7.90 (d, J = 8.4 Hz, 1H), 7.57 (d, J = 8.4 Hz, 2H), 7.38 (d, J= 15.6 Hz, 1H), 6.77 (s, 1H), 6.76 (d, J = 8.4 Hz, 1H), 6.70 (d, J = 8.4 Hz, 2H), 3.44-3.81 (m, 4H), 3.06 (s, 6H), 1.24 (t, J = 6.6 Hz, 3H), 1.22 (t, J = 6.6 Hz, 3H). ^{13}C NMR (150 MHz, $CDCl_3$) δ 192.5, 165.0, 157.2, 153.1, 152.3, 146.4, 130.8 (2C), 130.3, 122.3, 117.6, 114.3, 112.5, 111.7(2C), 110.7, 42.3, 42.0, 40.1 (2C),

14.2, 13.3. MS m/z: 383.2 $[M+H]^+$.

4.1.3.4. (*E*)-4-(3-(4-(dimethylamino)phenyl)acryloyl)-3-hydroxyphenyl pyrrolidine-1-carboxylate (6c)

Compound **3a** and **5c** were processed as above to afford product **6c**. Elution with petroleum ether/acetone = 2:1 and further recrystallization with EtOH gave **6c** as a yellow solid, 97.9% HPLC purity, mp 168.5-170.1 °C, yield 42.5%. ^{1}H NMR (600 MHz, $CDCl_3$) δ 13.42 (s, 1H), 7.90 (d, J = 15.6 Hz, 1H), 7.89 (d, *J* = 8.4 Hz, 1H), 7.57 (d, *J* = 8.4 Hz, 2H), 7.39 (d, *J* = 15.6 Hz, 1H), 6.79 (s, 1H), 6.78 (d, *J* = 8.4 Hz, 1H), 6.70 (d, *J* = 8.4 Hz, 2H), 3.56 (t, *J* = 6.6 Hz, 2H), 3.50 (t, *J* = 6.6 Hz, 2H), 3.06 (s, 6H), 1.99-1.93 (m, 4H). ^{13}C NMR (100 MHz, $CDCl_3$) δ 192.5, 165.1, 157.0, 152.3 (2C), 146.4, 130.8 (2C), 130.3, 122.3, 117.6, 114.3, 112.5, 111.8 (2C), 110.7, 46.5, 46.4, 40.1 (2C), 25.7, 24.9. MS m/z: 381.5 $[M+H]^+$.

4.1.3.5. (*E*)-4-(3-(4-(dimethylamino)phenyl)acryloyl)-1,3-phenylene bis(pyrrolidine-1-carboxylate) (7c)

Compound **3a** and **5c** were processed as above to afford product **7c**. Elution with petroleum ether/acetone = 2:1 gave **7c** as a yellow solid, 98.3% HPLC purity, mp 89.6-90.7 °C, yield 41.2%. ^{1}H NMR (400MHz, $CDCl_3$) δ 7.63 (d, *J* = 8.4 Hz, 1H), 7.52 (d, *J* = 16.0 Hz, 1H), 7.45 (d, *J* = 8.4 Hz, 2H), 7.15 (s, 1H), 7.11 (d, *J* = 8.4 Hz, 1H), 6.94 (d, *J* = 16.0 Hz, 1H), 6.66 (d, *J* = 8.4 Hz, 2H), 3.55 (t, *J* = 5.6 Hz, 2H), 3.49 (t, *J* = 5.6 Hz, 2H), 3.43 (t, *J* = 5.6 Hz, 2H), 3.36 (t, *J* = 5.6 Hz, 2H), 1.99-1.75 (m, 8H). ^{13}C NMR (150 MHz, CDCl3) δ 191.6, 153.6 (2C), 152.3 (2C), 149.7, 145.6, 130.2 (2C), 130.1 (2C), 121.3 (2C), 118.4, 117.0, 112.0 (2C), 46.4 (2C), 46.3 (2C), 40.3 (2C), 25.8, 25.6, 24.9, 24.8. MS m/z: 478.5 $[M+H]^+$.

4.1.3.6. (*E*)-4-(3-(4-(dimethylamino)phenyl)acryloyl)-3-hydroxyphenyl piperidine-1-carboxylate (6d)

Compound **3a** and **5d** were processed as above to afford product **6d**. Elution with petroleum ether/acetone = 3:1 and further recrystallization with EtOH gave **6d** as a yellow solid, 98.5% HPLC purity, mp 192.4-193.5 °C, yield 41.2%. ^{1}H NMR (400 MHz, $CDCl_3$) δ 13.42 (s, 1H), 7.91 (d, *J* = 14.8 Hz, 1H), 7.90 (d, *J* = 8.8 Hz, 1H), 7.57 (d, *J* = 8.8 Hz. 2H), 7.39 (d, *J* = 14.8 Hz, 1H), 6.76 (s, 1H), 6.71 (d, *J* = 8.8 Hz, 3H), 3.60 (s, 2H), 3.52 (s, 2H), 3.07 (s, 6H), 1.65 (s, 6H). ^{13}C NMR (100 MHz, $CDCl_3$) δ 192.5, 165.0, 157.2, 152.6, 152.3, 146.4, 130.8 (2C), 130.3, 122.3, 117.7, 114.3,

112.5, 111.8 (2C), 110.8, 45.7, 45.1, 40.1 (2C), 25.9, 25.5, 24.2. MS m/z: 395.3 $[M+H]^+$.

4.1.3.7. (*E*)-4-(3-(4-(dimethylamino)phenyl)acryloyl)-1,3-phenylene bis(piperidine-1-carboxylate) (7d)

Compound **3a** and **5d** were processed as above to afford product **7d**. Elution with petroleum ether/acetone = 3:1 gave **7d** as a yellow solid, 97.3% HPLC purity, mp 79.2-80.7 °C, yield 41.9%. ^{1}H NMR (400 MHz, $CDCl_3$) δ 7.62 (d, J = 8.4 Hz, 1H), 7.58 (d, J = 16.0 Hz, 1H), 7.46 (d, J = 8.4 Hz, 2H), 7.08 (d, J = 8.4 Hz, 1H), 7.07 (s, 1H), 6.90 (d, J = 16.0 Hz, 1H), 6.68 (d, J = 8.4 Hz, 2H), 3.76 (s, 2H), 3.67 (s, 2H), 3.58 (s, 2H), 3.37 (s, 2H), 3.06 (s, 6H), 2.31 (s, 6H), 1.81 (s, 6H). MS m/z: 506.3 $[M+H]^+$.

4.1.3.8. (*E*)-4-(3-(4-(dimethylamino)phenyl)acryloyl)-3-hydroxyphenyl morpholine-4-carboxylate (6e)

Compound **3a** and **5e** were processed as above to afford product **6e**. Elution with petroleum ether/acetone = 3:1 and further recrystallization with EtOH gave **6e** as a yellow solid, 97.9% HPLC purity, mp 182.9-183.4 °C, yield 63.6%. ^{1}H NMR (600 MHz, $CDCl_3$) δ 13.45 (s, 1H), 7.92 (d, J = 16.2 Hz, 1H), 7.91 (d, J = 8.4 Hz, 1H), 7.57 (d, J = 8.4 Hz, 2H), 7.39 (d, J = 16.2 Hz, 1H), 6.77 (s, 1H), 6.74 (d, J = 8.4 Hz, 1H), 6.70 (d, J = 8.4 Hz, 2H), 3.76 (s, 4H), 3.67 (s, 2H), 3.59 (s, 2H), 3.067 (s, 6H). ^{13}C NMR (150 MHz, $CDCl_3$) δ 192.5, 165.0, 156.7, 152.6, 152.3, 146.6, 130.9 (2C), 130.4, 122.2, 118.0, 114.2, 112.4, 111.8 (2C), 110.8, 66.6, 66.4, 45.0, 44.1, 40.1 (2C). MS m/z: 397.2 $[M+H]^+$.

4.1.3.9. (*E*)-4-(3-(4-(dimethylamino)phenyl)acryloyl)-1,3-phenylene bis(morpholine-4-carboxylate) (7e)

Compound **3a** and **5e** were processed as above to afford product **7e**. Elution with petroleum ether/acetone = 3:1 gave **7e** as a yellow solid, 98.3% HPLC purity, mp 82.7-84.3 °C, yield 28.3%. ^{1}H NMR (600 HMz, $CDCl_3$) 7.63 (d, J = 8.4 Hz, 1H), 7.50 (d, J = 15.6 Hz, 1H), 7.45 (d, J = 8.4 Hz, 2H), 7.12 (s, 1H), 7.10 (d, J = 8.4 Hz, 1H), 6.90 (d, J = 15.6 Hz, 1H), 6.66 (d, J = 8.4 Hz, 2H), 3.75 (s, 4H), 3.67 (s, 2H), 3.58 (s, 2H), 3.51 (s, 6H), 3.45 (s, 2H), 3.04 (s, 6H). ^{13}C NMR (100 Hz, $CDCl_3$) δ 191.5, 153.1, 152.7, 152.6, 152.1, 149.4, 146.4, 130.5, 130.4 (2C), 130.3, 121.9, 120.7, 118.7, 117.0, 111.7 (2C), 66.6, 66.4 (2C), 66.3, 44.9 (2C), 44.1 (2C), 40.0 (2C). MS m/z: 510.2 $[M+H]^+$.

4.1.3.10. (*E*)-4-(3-(4-(dimethylamino)phenyl)acryloyl)-3-hydroxyphenyl ethyl(methyl)

carbamate (6f)

Compound **3a** and **5f** were processed as above to afford product **6f**. Elution with petroleum ether/acetone = 3:1 and further recrystallization with EtOH gave 6F as a yellow solid, 98.5% HPLC purity, mp 203.5-205.1 °C, yield 55.8%. ^{1}H NMR (400 MHz, $CDCl_3$) δ 13.44 (s, 1H), 7.91 (d, J = 14.8 Hz, 1H), 7.90 (d, J = 8.8 Hz, 1H), 7.57 (d, J = 8.4 Hz, 2H), 7.39 (d, J = 14.8 Hz, 1H), 6.77 (s, 1H), 6.75 (d, J = 8.8 Hz, 1H), 6.70 (d, J = 8.4 Hz, 2H), 3.49-3.39 (m, 2H), 3.06 (s, 6H), 3.00 (s, 1.5H), 2.84 (s, 1.5H), 1.31-1.23 (m, 3H). ^{13}C NMR (100 Hz, CDCl3) δ 192.6, 165.0, 157.1, 152.3 (2C), 146.4, 130.8 (2C), 130.3, 122.3, 117.7, 114.3, 112.5, 111.8 (2C), 110.8, 44.2 (2C), 40.1 (2C), 13.2. MS m/z: 369.2 $[M+H]^+$.

4.1.3.11. (*E*)-4-(3-(4-(dimethylamino)phenyl)acryloyl)-3-hydroxyphenyl 4-methylpiperazine-1-carboxylate (6g)

Compound **3a** and **5g** were processed as above to afford product **6g**. Elution with petroleum ether/acetone = 1:1 and further recrystallization with EtOH gave **6g** as a yellow solid, 97.5% HPLC purity, mp 157.5-158.7 °C, yield 59.6%. ^{1}H NMR (400 MHz, $CDCl_3$) δ 13.45 (s, 1H), 7.92 (d, J = 8.4 Hz, 1H), 7.91 (d, J = 14.4 Hz, 1H), 7.57 (d, J = 8.8 Hz, 2H), 7.39 (d, J = 14.4 Hz, 1H), 6.76 (s, 1H), 6.75 (d, J = 8.4 Hz, 1H), 6.70 (d, J = 8.8 Hz, 2H), 3.72 (s, 2H), 3.63 (s, 2H), 3.07 (s, 6H), 2.51 (s, 4H), 2.38 (s, 3H). ^{13}C NMR (100 MHz, $CDCl_3$) δ 192.5, 165.0, 156.8, 152.5, 152.3, 146.5, 130.9 (2C), 130.4, 122.2, 117.9, 114.2, 112.4, 111.8 (2C), 110.8, 54.6, 54.5, 46.0, 44.4, 43.7, 40.1 (2C). MS m/z: 410.3 $[M+H]^+$.

4.1.3.12. (*E*)-4-(3-(4-(dimethylamino)phenyl)acryloyl)-3-hydroxyphenyl 4-ethylpiperazine-1-carboxylate (6h)

Compound **3a** and **5h** were processed as above to afford product **6h**. Elution with petroleum ether/acetone = 1:1 and further recrystallization with EtOH gave **6h** as a yellow solid, 98.2% HPLC purity, mp 189.2-191.3 °C, yield 53.2%. ^{1}H NMR (400 MHz, $CDCl_3$) δ 13.45 (s, 1H), 7.91 (d, J = 8.8 Hz, 1H), 7.90 (d, J = 15.2 Hz, 1H), 7.57 (d, J = 8.8 Hz, 2H), 7.39 (d, J = 15.2 Hz, 1H), 6.76 (d, J = 8.8 Hz, 1H), 6.72 (d, J = 8.8 Hz, 2H), 6.69 (s, 1H), 3.69 (s, 2H), 3.61 (s, 2H), 3.06 (s, 6H), 2.52-2.45 (m, 6H), 1.13 (t, J = 7.2 Hz, 3H). ^{13}C NMR (150 MHz, $CDCl_3$) δ 192.6, 165.0, 156.9, 152.5, 152.3, 146.5, 130.8 (2C), 130.4, 122.3, 117.8, 114.2, 112.4, 111.8 (2C), 110.8, 52.5, 52.3 (2C), 44.6, 44.0, 40.1 (2C), 12.0. MS m/z: 424.3 $[M+H]^+$.

4.1.3.13. (*E*)-4-(3-(4-(dimethylamino)phenyl)acryloyl)-3-hydroxyphenyl 4-benzylpiperazine-1-carboxylate (6i)

Compound **3a** and **5i** were processed as above to afford product **6i**. Elution with petroleum ether/acetone = 1:1 and further recrystallization with EtOH gave **6i** as a yellow solid, 98.1% HPLC purity, mp 132.1-133.5 ℃, yield 52.9%. ^{1}H NMR (400 MHz, $CDCl_3$) δ 13.44 (s, 1H), 7.91 (d, J = 15.2 Hz, 1H), 7.90 (d, J = 8.8 Hz, 1H), 7.57 (d, J = 8.8 Hz, 2H), 7.39 (d, J = 15.2 Hz, 1H), 7.35-7.28 (m, 5H), 6.76 (s, 1H), 6.74 (d, J = 8.8 Hz, 1H), 6.70 (d, J = 8.8 Hz, 2H), 3.67 (s, 2H), 3.57 (s, 4H), 3.07 (s, 6H), 2.51 (t, J = 6.4 Hz, 4H). ^{13}C NMR (150 MHz, CDCl3) δ 192.5, 165.0, 156.9, 152.5, 152.3, 146.5, 130.8 (2C), 130.4, 129.2 (2C), 128.4 (2C), 127.4, 122.3, 117.8, 114.2, 112.4, 112.3, 111.8 (2C), 110.8, 62.9, 52.7, 52.5, 44.5, 43.9, 40.4 (2C). MS m/z: 486.3 $[M+H]^+$.

4.1.3.14. (*E*)-4-(3-(4-(diethylamino)phenyl)acryloyl)-3-hydroxyphenyl pyrrolidine-1-carboxylate (8b)

Compound **3b** and **5c** were processed as above to afford product **8b**. Elution with petroleum ether/acetone = 2:1 and further recrystallization with EtOH gave **8b** as a yellow solid, 97.5% HPLC purity, mp 132.0-133.6 ℃, yield 45.2%. ^{1}H NMR (400MHz, $CDCl_3$) δ 13.50 (s, 1H), 7.90 (d, J = 9.6 Hz, 1H), 7.89 (d, J = 15.2 Hz, 1H), 7.55 (d, J = 8.8 Hz, 2H), 7.36 (d, J = 15.2 Hz, 1H), 6.78 (d, J = 9.6 Hz, 1H), 6.77 (s, 1H), 6.66 (d, J = 8.8 Hz, 2H), 3.56 (t, J = 6.4 Hz, 2H), 3.49 (t, J = 6.4 Hz, 2H), 3.42 (q, J = 7.2 Hz, 4H), 1.99-1.92 (m, 4H), 1.21 (t, J = 7.2 Hz, 6H). ^{13}C NMR (100MHz, $CDCl_3$) δ 192.4, 165.0, 156.9, 151.9, 150.0, 146.4, 131.2, 130.3, 121.4, 117.6, 113.5, 112.4, 111.2 (2C), 110.6, 46.5, 46.4, 44.5 (2C), 25.7, 24.9, 12.5 (2C). MS m/z: 409.2 $[M+H]^+$.

4.1.3.15. (*E*)-3-hydroxy-4-(3-(4-(pyrrolidin-1-yl)phenyl)acryloyl)phenyl pyrrolidine-1-carboxylate (8c)

Compound **3c** and **5c** were processed as above to afford product **8c**. Elution with petroleum ether/acetone = 2:1 and further recrystallization with EtOH gave **8c** as a yellow solid, 97.8% HPLC purity, mp 154.8-155.4 ℃, yield 56.9%. ^{1}H NMR (400MHz, $CDCl_3$) δ 13.50 (s, 1H), 7.91 (d, J = 14.4 Hz, 1H), 7.90 (d, J = 8.4 Hz, 1H), 7.56 (d, J = 8.4 Hz, 2H), 7.37 (d, J = 14.4 Hz, 1H), 6.78 (s, 1H), 6.77 (d, J = 8.4 Hz, 1H), 6.56 (d, J = 8.4, 2H), 3.56 (t, J = 6.4, 2H), 3.49 (t, J = 6.4, 2H), 3.37 (t, J = 6.4, 4H), 2.06-2.03 (m, 4H), 1.99-1.92 (m, 4H). ^{13}C NMR (100 MHz, $CDCl_3$) δ 192.4, 165.0,

156.9, 149.9 (2C), 146.7, 131.0 (2C), 130.3, 121.7, 117.7, 113.5, 112.4, 111.7 (2C), 110.6, 47.5 (2C), 46.5, 46.4, 25.7, 25.4 (2C), 24.9. MS m/z: 407.3 $[M+H]^+$.

4.1.3.16. (*E*)-3-hydroxy-4-(3-(4-(piperidin-1-yl)phenyl)acryloyl)phenyl pyrrolidine-1-carboxylate (8d)

Compound **3d** and **5c** were processed as above to afford product **8d**. Elution with petroleum ether/acetone = 2:1 and further recrystallization with EtOH gave **8d** as a yellow solid, 98.8% HPLC purity, mp 145.7-148.0 ℃, yield 47.2%. ^{1}H NMR (400MHz, $CDCl_3$) δ 13.26 (s, 1H), 7.80 (d, J = 9.2 Hz, 1H), 7.78 (d, J = 15.2 Hz, 1H), 7.45 (d, J = 9.2 Hz, 2H), 7.31 (d, J = 15.2 Hz, 1H), 6.79 (d, J = 9.2 Hz, 2H), 6.68 (d, J = 9.2 Hz, 1H), 6.67 (s, 1H), 3.46 (t, J = 6.8 Hz, 2H), 3.39 (t, J = 6.8 Hz, 2H), 3.24(t, J = 5.6 Hz, 4H), 1.89-1.82 (m, 4H), 1.59-1.56 (m, 6H). ^{13}C NMR (100 MHz, $CDCl_3$) δ 192.6, 165.0, 157.1, 153.3 (2C), 145.9, 130.7 (2C), 130.4, 123.8, 117.6, 115.2, 114.5, 112.5, 110.7 (2C), 48.8 (2C), 46.5, 46.4, 25.7, 25.4 (2C), 24.9, 24.3. MS m/z: 421.2 $[M+H]^+$.

4.1.3.17. (*E*)-3-hydroxy-4-(3-(4-morpholinophenyl)acryloyl)phenyl pyrrolidine-1-carboxylate (8e)

Compound **3e** and **5c** were processed as above to afford product **8e**. Elution with petroleum ether/acetone = 2:1 and further recrystallization with EtOH gave **8e** as a yellow solid, 97.9% HPLC purity, mp 154.8-155.4 ℃, yield 56.9%. ^{1}H NMR (600MHz, $CDCl_3$) δ 13.27 (s, 1H), 7.92 (d, J = 8.4 Hz, 1H), 7.88 (d, J = 16.2 Hz, 1H), 7.59 (d, J = 8.4 Hz, 1H), 7.45 (d, J = 16.2 Hz, 1H), 7.37 (d, J = 8.4 Hz, 1H), 6.95 (d, J = 8.4 Hz, 1H), 6.90 (d, J = 7.8 Hz, 1H), 6.80 (s, 1H), 6.79 (d, J = 7.8 Hz, 1H), 3.87 (t, J = 4.8 Hz, 4H), 3.52 (t, J = 4.8 Hz, 4H), 3.29 (t, J = 4.8 Hz, 2H), 3.19 (t, J = 4.8 Hz, 2H), 1.99-1.92 (m, 4H). MS m/z: 423.2 $[M+H]^+$.

4.2. Biological evaluation

4.2.1. *In vitro* inhibition of ChE

The assay followed the method of Ellman *et al*, using purified AChE from *E. electricus* (Sigmae-Aldrich Co.) and BuChE from rat serum.[24] For the measurement of *E. electricus* AChE inhibition assays, acetylthiocholine iodide (1 mmol/L, 30 μL), phosphate-buffered solution (0.1 mmol/L, pH = 8.0, 40 μL), *Ee*AChE (0.05 U/mL, final concentration, 10 μL) and different concentrations of test compounds (20 μL) were added in 96-well plates successively. The mixture

was incubated at 37 °C for 15min. Then 5,5′-dithiobis-2-nitrobenzoic acid (DTNB, 0.2%, 30 μL) was added to yield the yellow anion of 5-thio-2-nitrobenzoic acid. Activity was determined by measuring the increase in absorbance at 412 nm, using Varioskan Flash Multimode Reader (Thermo Scientific). For BuChE inhibition assays, butyrylthiocholine iodide (1 mmol/L, 30 μL), phosphate-buffered solution (0.1 mmol/L, pH = 7.4, 40 μL), 25 % serum (10 μL) were used and changes in absorbance were detected at 405 nm. The other procedures were the same as above. Each concentration was assayed in triplicate. Blanks containing all components except AChE were carried out. The percent inhibition was calculated by the following expression: $(1 - A_i/A_c) \times 100$, where A_i and A_c are the absorbance obtained for ChE in the presence and absence of inhibitors, respectively, after subtracting the respective background. IC_{50} values were calculated as the concentration of compound that produces more than 50% AChE or BuChE activity inhibition.

4.2.2. Kinetic characterization of AChE inhibition

Kinetic characterization of AChE inhibition was conducted based on an established method using purified AChE from *E. electricus* (*Ee*AChE) (Sigma–Aldrich Co.).[28,29] The assay solution (100 μL) consists of 0.1 M phosphate buffer (pH 8.0), with the addition of 10 μL of 0.5 U/mL *Ee*AChE, 30 μL of 0.2% DTNB and 20 μL of substrate ATCh (acetylthiocholine iodide). Three different concentrations of inhibitors were added to the assay solution and preincubated for 15 min at 37 °C with the *Ee*AChE followed by the addition of substrate in different concentrations. Kinetic characterization of the hydrolysis of ATCh catalyzed by *Ee*AChE was done spectrometrically at 412 nm. The parallel control experiments were performed without inhibitor in the assay. The plots were assessed by a weighted least square analysis that assumed the variance of ν to be a constant percentage of ν for the entire data set. Slopes of these reciprocal plots were then plotted against the concentration of the inhibitors in a weighted analysis.

4.2.3. Oxygen radical absorbance capacity (ORAC-FL) assay

The antioxidant activity was determined by the oxygen radical absorbance capacity-fluorescein (ORAC-FL) assay.[30] The ORAC-assay measured antioxidant scavenging activity against peroxyl radical induced by 2,2′-Azobis(amidino propane) dihydrochloride (AAPH) at 37°C. The reaction was carried out in 75 μL phosphate buffer (pH 7.4) and the final reaction mixture was 200 μL. Antioxidant (20 μL) and fluorescein (FL) (120 μL, 150 nM final concentration) were placed in

the wells of a black 96 well plate and the mixture was incubated for 15 min at 37°C. Then AAPH solution (60 µL; 12 mM final concentration) was added rapidly. The plate was immediately placed into a Varioskan Flash Multimode Reader (Thermo Scientific) and the fluorescence was measured every 60 seconds for 90 minutes with exitation at 485 nm and emission at 535 nm. 6-Hydroxy-2,5,7,8-tetramethylchroman-2-carboxylic acid (Trolox) was used as standard (1-8 µM, final concentration). A blank (FL+AAPH) using phosphate buffer instead of antioxidant and trolox calibration were carried out in each assay. The samples were measured at different concentrations (1-10 µM). All reaction mixtures were prepared duplicate and at least three independent runs were performed for each sample. Fluorescence measurements were normalized to the curve of the blank (without antioxidant). From the normalized curves, the area under the fluorescence decay curve (AUC) was calculated as: $AUC = \sum_{i=1}^{i=90} (f_i / f_o)$, where f_0 is the initial fluorescence reading at 0 min and f_i is the fluorescence reading at time i. The net AUC was calculated by the expression $AUC_{sample} - AUC_{blank}$. The ORAC-FL values were calculated: [(AUC $_{sample}$ – AUC_{blank})/(AUC $_{trolox}$ – AUC $_{blank}$)]×[(concentration of trolox/concentration of sample)] and the ORAC-FL value of tested compounds expressed as trolox equivalents.

4.2.4. Metal-chelating studies[29]

Compound **6c** was tested as a metal chelator using difference UV−vis spectra, recorded with a Varioskan Flash Multimode Reader (Thermo Scientific).The wavelength ranged from 200 to 600 nm. Numerical subtraction of the spectra of the metal ($CuCl_2$, $ZnCl_2$, $AlCl_3$, and $FeSO_4$) alone and the compound alone from the spectra of the mixture gave the difference UV−vis spectra due to complex formation, after incubating for 30 min at room temperature. The final concentrations of tested compound and metals were 37.5 µM and the final volume of reaction mixture was 200 µL. The molar ratio method was performed to determine the stoichiometry of the compound-Cu^{2+} by titrating the methanol solution of compound **6c** with ascending amounts of $CuCl_2$. The UV spectra were recorded and treated by numerical subtraction of $CuCl_2$ and **6c** at corresponding concentrations, plotted versus the mole fraction of **6c**.

4.2.5. *In vitro* inhibition of self and Cu^{2+}-induced A$\beta_{1\text{-}42}$ aggregation

Inhibition of A$\beta_{1\text{-}42}$ aggregation was measured using a Thioflavin T (ThT)-binding assay.[27,35,36] Experiments were performed by incubating A$\beta_{1\text{-}42}$ dissolved in 1,1,1,3,3,3-hexafluoro-2-propanol

(HFIP) (1 mg/mL) for 24 h at room temperature. Then, the solvent was evaporated. After incubation, the HFIP pretreated A$\beta_{1\text{-}42}$ were primarily diluted in dry DMSO to a concentration of 200 μM and was kept at –80 °C, in order to remain a stable stock solution. Before use, solutions of test compounds were prepared in DMSO in 2.5 mM for storage and diluted with phosphate buffer solution (pH 7.4). For the self-induced A$\beta_{1\text{-}42}$ aggregation assay, A$\beta_{1\text{-}42}$ (20 μL, 25 μM, final concentration) was incubated with 20 μL of test compounds (25 μM, final concentration) in 50 mM phosphate buffer solution (pH 7.40) at 37 °C for 24 h. Next, 50 mM glycine-NaOH buffer (pH 8.5) containing 160 μL of 5 μM ThT was added. Fluorescence signal was measured (λ_{exc} = 446 nm; λ_{em} = 490 nm) on a Varioskan Flash Multimode Reader (Thermo Scientific). The percent inhibition of aggregation was calculated using the following equation: $(1\text{-}IF_i/IF_c) \times 100$, in which IF_i and IF_c are the fluorescence intensities obtained for for absorbance in the presence and absence of inhibitors after subtracting the background, respectively. The background activity was determined from wells containing all components except A$\beta_{1\text{-}42}$, which were replaced by a phosphate buffer solution (pH 7.40) and each assay was run in triplicate.

To study the effects of the Cu^{2+}-induced A$\beta_{1\text{-}42}$ aggregation, solutions of Cu^{2+} were prepared from standards to final concentrations of 75 μM using the HEPES buffer at pH 6.6 (20 mM, 150 mM NaCl). Aβ_{1-42} (20 μL, 25 μM,) was incubated with Cu^{2+} (20 μL, 25 μM) in HEPES buffer at pH 6.6, without or with the tested compound (20 μL, 25 μM, final concentration). The incubation was performed at 37 °C for 24 h. After incubation, 190 μL of 50 mM glycine−NaOH buffer (pH 8.5) containing 5 μM thioflavin T was added. The detection was carried out as in the previous procedure and each assay was run in triplicate.

4.2.6. *In vitro* inhibition of monoamine oxidase[37-39]

Recombinant human MAO-A and -B were obtained from commercial sources (Sigma–Aldrich Co.). The enzymatic reactions were conducted in potassium phosphate buffer (100 mM, pH = 7.4, made isotonic with KCl 20.2 mM) to a final volume of 500 μL, and contained kynuramine (45 μL for MAO-A and 30 μL for MAO-B), various concentrations of the test inhibitors (0-100 μL) and lower than 4% DMSO as cosolvent. The reactions were initiated by the addition of MAO-A or -B (7.5 μg/mL) and were subsequently incubated for 30 min at 37 °C. The reactions were terminated by the addition of 400 μL NaOH (2 N) and 1000 μL water, centrifuged for 10 min at 16000 g and the

concentrations of 4-hydroxyquinoline in the supernatants were measured spectrofluorometrically (λ_{ex}= 310 nm; λ_{em}= 400 nm), using the Varioskan Flash Multimode Reader (Thermo Scientific). A linear calibration curve was constructed by preparing samples containing 4-hydroxyquinoline (0.047–1.56 μM) dissolved in 500 μL potassium phosphate buffer. Volumes of 400 μL NaOH (2 N) and 1000 μL water were added to each calibration standard. The appropriate control samples were included to confirm that the test inhibitors do not fluoresce or quench the fluorescence of 4-hydroxyquinoline under these assay conditions. IC_{50} values were estimated from sigmoidal dose–response curves (graphs of the initial rate of kynuramine oxidation versus the logarithm of inhibitor concentration). Each sigmoidal curve was constructed from six different inhibitor concentrations spanning at least three orders of magnitude. Data analyses were carried out with the Prism 5 software package (GraphPad) employing the one site competition model. The background activity was determined from wells containing all components except the *h*MAO isoforms, which were replaced by a sodium phosphate buffer solution. IC_{50} values were determined in triplicate and are expressed as mean ± standard deviation (SD).

4.2.7. Docking study[35]

The crystal structures of AChE complexed with donepezil (code ID: 1EVE) and MAO-B (code ID: 2V60) were obtained from the Protein Data Bank after eliminating the original inhibitors and water molecules. First, in the PDB crystallographic structures any co-crystallized solvent and the ligand were removed. Then, proper bonds, bond orders, hybridization and charges were assigned using protein model tool in Discovery Studio, version 2.5, software package. CHARMm force field was applied using the receptore ligand interactions tool in Discovery Studio, version 4.5, software package. The ligand binding site was defined as 13.4 Å from the original ligand. Docking studies were performed using Autodock 4.2 program and each docked system was performed by 30 runs of the Autodock search by the Lamarckian genetic algorithm (LGA).

4.2.8. *In vitro* blood-brain barrier permeation assay

The blood-brain barrier penetration of compound **6c** was evaluated using the parallel artificial membrane permeation assay of the blood-brain barrier (PAMPA-BBB).[35,40,41] The donor plate (MATRNPS50) and the acceptor plate (PVDF membrane, pore size 0.45 μm, MAIPN4550) were purchased from Millipore. Porcine brain lipid (PBL) was purchased from Avanti Polar Lipids and

commercial drugs were purchased from Sigma and Alfa Aesar. Filter PDVF membrane units (diameter 25 mm, pore size 0.45 μm) from Pall Corporation were used to filter the samples. Compound **6c** was dissolved in DMSO at 5 mg/mL and diluted 50-fold in PBS/EtOH (70:30) to a final concentration of 100 μg/mL. Then the diluted compound solution (100 μg/mL, 350 μL) was added to the donor wells. The acceptor wells were filled with 200 μL of PBS/EtOH (70:30) and the filter membrane was coated with PBL in dodecane (selected empirically as 4 μL volume of 20 μg/mL PBL in dodecane) and. The acceptor filter plate was carefully put on the donor plate to form a sandwich (consisting of the aqueous donor with test compound on the bottom, lipid membrane in the middle and the aqueous acceptor on the top), which was left undisturbed for 18 h at 25 °C. After incubation, the donor and acceptor plates were separated carefully and the concentration of drug in the donor and acceptor wells was determined using the Varioskan Flash Multimode Reader (Thermo Scientific). Every sample was analyzed at ten wavelengths in four wells and in at least three independent runs. P_e was calculated using the following expression:

$$P_e = -\ln [1 - C_A(t)/C_{equilibrium}]/[A \times (1/V_D + 1/V_A) \times t]$$

$$C_{equilibrium} = [C_D(t) \times V_D + C_A(t) \times V_A]/(V_D + V_A)$$

Where P_e is permeability in the unit of cm/s. A is effective filter area and t is the permeation time. V_D is the volume of donor well and V_A is the volume of acceptor well. $C_A(t)$ is the compound concentration in acceptor well at time t, and $C_D(t)$ is the compound concentration in donor well at time t. Results are given as the mean ± SD. In the experiment, 11 quality control drugs of known BBB permeability were included to validate the analysis set. A plot of the experimental data versus literature values gave a strong linear correlation, P_e(exp.) = 0.8792 × P_e(bibl.)−0.0616 (R^2 = 0.9555). From this equation and taking into account the limit established by Di *et al.* for BBB permeation, we determined that compounds with P_e values above 3.46 × 10^{-6} cm/s could cross the BBB.

Supplementary data

Supplementary data (the ^{1}H NMR and ^{13}C NMR spectra of target compounds) associated with this article can be found, in the online version.

References and notes

1. Benhamu, B.; Martin-Fontecha, M.; Vazquez-Villa, H.; Pardo, L.; Lopez-Rodriguez, M. L. *J. Med. Chem.* **2014**, *57*, 7160.

2. Martin, P.; Adelina, C.; Martin, K.; Maëlenn, G.; Maria K. *World Alzheimer Report.* 2016, pp.1-140

3. Scarpini, E.; Scheltens, P.; Feldman, H. *Lancet Neurol.* **2003**, *2*, 539.

4. Kumar, A.; Singh, A.; Ekavali. *Pharmacol Rep.* **2015**, *67*, 195.

5. Cummings, J. L.; Doody, R.; Clark, C. *Neurology.* **2007**, *69*, 1622.

6. Jameson, L. P.; Dzyuba, S. V. *Bioorg. Med. Chem. Lett.* **2013**, *23*, 1732.

7. Sanchez, L.; Madurga, S.; Pukala, T.; Vilaseca, M.; Lopez-Iglesias, C.; Robinson, C. V.; Giralt, E.; Carulla, N. *J. Am. Chem. Soc.* **2011**, *133*, 6505.

8. Curtain, C. C.; Ali, F.; Volitakis, I.; Cherny, R. A.; Norton, R. S.; Beyreuther, K.; Barrow, C. J.; Masters, C. L.; Bush, A. I.; Barnham, K. J. *J. Biol. Chem.* **2001**, *276*, 20466.

9. Sang, Z.; Li, Y.; Qiang, X.; Xiao, G.; Liu, Q.; Tan, Z.; Deng, Y. *Bioorg. Med. Chem.* **2015**, *23*, 668.

10. Carradori, S.; Petzer, J. P. *Expert. Opin. Ther. Pat.* **2015**, *25*, 91.

11. Xie, S.; Chen, J.; Li, X.; Su, T.; Wang, Y.; Wang, Z.; Huang, L.; Li, X. *Bioorg. Med. Chem.* **2015**, *23*, 3722.

12. Riederer, P.; Danielczyk, W.; Grunblatt, E. *Neurotoxicology.* **2004**, *25*, 271.

13. Chao, X.; He, X.; Yang, Y.; Zhou, X.; Jin, M.; Liu, S.; Cheng, Z.; Liu, P.; Wang, Y.; Yu, J.; Tan, Y.; Huang, Y.; Qin, J.; Rapposelli, S.; Pi, R. *Bioorg. Med. Chem. Lett.* **2012**, 22, 6498.

14. Xie, S.; Wang, X.; Li, J.; Yang, L.; Kong, L. *Eur. J. Med. Chem.* **2013**, 64, 540.

15. Liu, H.; Liu, X.; Fan, H.; Tang, J.; Gao, X.; Liu, W. *Bioorg. Med. Chem.* **2014**, *22*, 6124.

16. Choi, J. W.; Jang, B. K.; Cho, N. C.; Park, J. H.; Yeon, S. K.; Ju, E. J.; Lee, Y. S.; Han, G.; Pae, A. N.; Kim, D. J.; Park, K. D. *Bioorg. Med. Chem.* **2015**, *23*, 6486.

17. Fuchigami, T.; Yamashita, Y.; Haratake, M.; Ono, M.; Yoshida, S.; Nakayama, M. *Bioorg. Med. Chem.* **2014**, *22*, 2622.

18. Bag, S.; Ghosh, S.; Tulsan, R.; Sood, A.; Zhou, W.; Schifone, C.; Foster, M.; LeVine, H., III; Torok, B.; Torok, M. *Bioorg. Med. Chem. Lett.* **2013**, *23*, 2614.

19. Ono, M.; Watanabe, R.; Kawashima, H.; Cheng, Y.; Kimura, H.; Watanabe, H.; Haratake, M.;

Saji, H.; Nakayama, M. *J. Med. Chem.* **2009**, *52*, 6394.

20. Chaudhaery, S. S.; Roy, K. K.; Shakya, N.; Saxena, G.; Sammi, S. R.; Nazir, A.; Nath, C.; Saxena, A. K. *J. Med. Chem.* **2010**, *53*, 6490.

21. Groner, E.; Ashani, Y.; Schorer-Apelbaum, D.; Sterling, J.; Herzig, Y.; Weinstock, M. *Mol. Pharmacol.* **2007**, *71*, 1610.

22. Lee, Y.; Fong, T. H.; Chen, H.; Chang, C.; Wang, Y.; Chern, C.; Chen, Y. *Molecules.* **2014**, *19*, 641.

23. Yuan, W.; Sang, Z.; Qiang, X.; Tan, Z.; Deng, Y. *Res. Chem. Intermed.* **2014**, *40*, 787.

24. Qiang, X.; Sang, Z.; Yuan, W.; Li, Y.; Liu, Q.; Bai, P.; Shi, Y.; Tan, Z.; Deng, Y. *Eur. J. Med. Chem.* **2014**, *76*, 314.

25. Schwarz, S.; Lucas, S. D.; Sommerwerk, S.; Csuk, R. *Bioorg. Med. Chem.* **2014**, *22*, 3370.

26. Yanovsky, I.; Finkin-Groner, E.; Zaikin, A.; Lerman, L.; Shalom, H.; Zeeli, S.; Weill, T.; Ginsburg, I.; Nudelman, A.; Weinstock, M. *J. Med. Chem.* **2012**, *55*, 10700.

27. Li, R.; Wang, X.; Hu, X.; Kong, L. *Bioorg. Med. Chem. Lett.* **2013**, *23*, 2636.

28. Liu, Q.; Qiang, X.; Li, Y.; Sang, Z.; Li, Y.; Tan, Z.; Deng, Y. *Bioorg. Med. Chem.* **2015**, *23*, 911.

29. Pan, W.; Hu, K.; Bai, P.; Yu, L.; Ma, Q.; Li, T.; Zhang, X.; Chen, C.; Peng, K.; Liu, W.; Sang, Z. *Bioorg. Med. Chem. Lett.* **2016**, 26, 2539.

30. Maalej, E.; Chabchoub, F.; Oset-Gasque, M. J.; Esquivias-Perez, M.; Gonzalez, M. P.; Monjas, L.; Perez, C.; de los Rios, C.; Rodriguez-Franco, M. I.; Iriepa, I.; Moraleda, I.; Chioua, M.; Romero, A.; Marco-Contelles, J.; Samadi, A. *Eur. J. Med. Chem.* **2012**, *54*, 750.

31. Sang, Z.; Qiang, X.; Li, Y.; Yuan, W.; Liu, Q.; Shi, Y.; Ang, W.; Luo, Y.; Tan, Z.; Deng Y. *Eur. J. Med. Chem.* **2015**, *94*, 348.

32. Liang, H.; Xiang, Z.; Ma, T.; Zhang, X.; Wu, J. *Chin. Pharm. J.* **2014**, *49*, 1939.

33, Wu, J.; Li, W.; Chen, L.; Chu, S.; Zhao, C.; Wei, T.; Yang, S.; Li, X. *Chin. J. Org. Chem.* **2012**, *32*, 2141.

34, M. Amélia, S.; Karam, C.; Silvia, C. *Coord. Chem. Rev.* **2016**, *327*, 287.

35. Li, Y.; Qiang, X.; Luo, L.; Li, Y.; Xiao, G.; Tan, Z.; Deng, Y. *Bioorg. Med. Chem.* **2016**, *24*, 2342.

36. Li, Y.; Qiang, X.; Li, Y.; Yang, X.; Luo, L.; Xiao, G.; Cao, Z.; Tan, Z.; Deng, Y. *Bioorg. Med. Chem. Lett.* **2016**, *26*, 2035.

37. Bolea, I.; Juarez-Jimenez, J.; de Los Rios, C.; Chioua, M.; Pouplana, R.; Luque, F. J.; Unzeta, M.; Marco-Contelles, J.; Samadi, A. *J. Med. Chem.* **2011**, *54*, 8251.

38. Xie, S.; Wang, X.; Jiang, N.; Yu, W.; Wang, K.; Lan, J.; Li, Z.; Kong, L. *Eur. J. Med. Chem.* **2015**, *95*, 153.

39. Strydom, B.; Malan, S. F.; Castagnoli, N., Jr.; Bergh, J. J.; Petzer, J. P. *Bioorg. Med. Chem.* **2010**, *18*, 1018.

40. Luo, Z.; Sheng, J.; Sun, Y.; Lu, C.; Yan, J.; Liu, A.; Luo, H. B.; Huang, L.; Li, X. *J. Med. Chem.* **2013**, *56*, 9089.

41. Di, L.; Kerns, E. H.; Fan, K.; McConnell, O. J.; Carter, G. T. *Eur. J. Med. Chem.* **2003**, *38*, 223.

Graphical Abstract

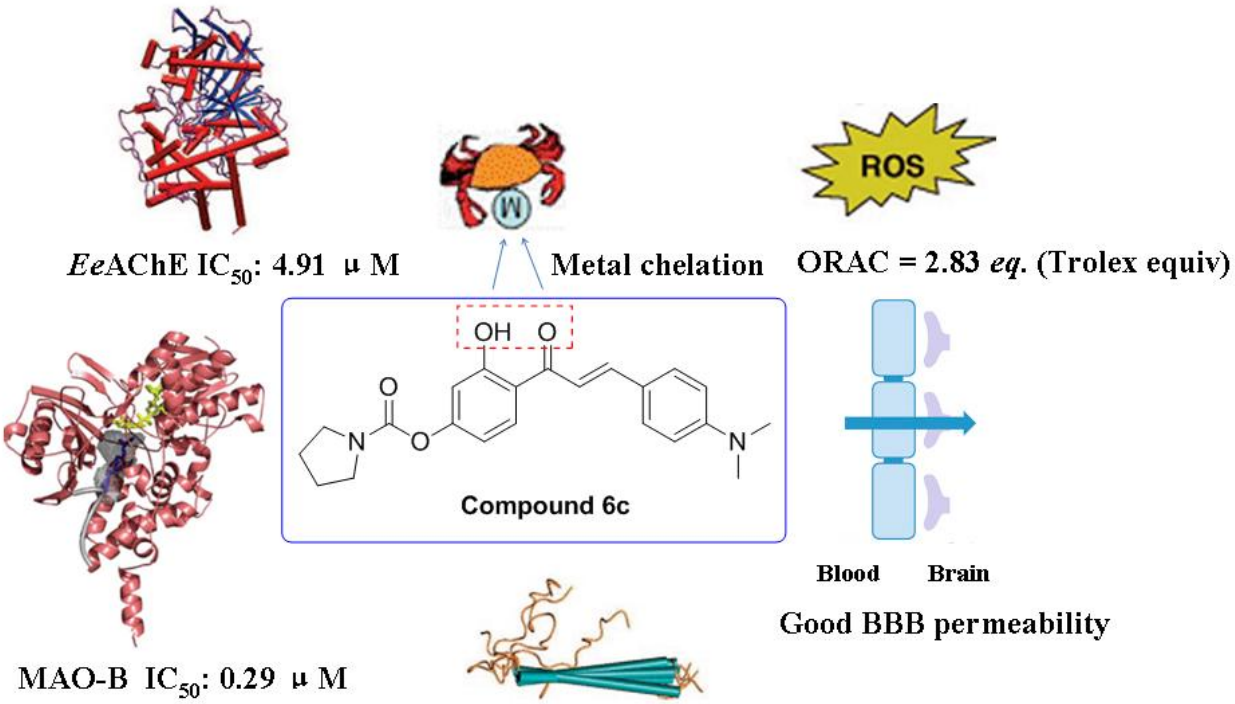

Self-induced A $\beta_{1\text{-}42}$ aggregation: 89.5% inhibition at 25 μ M
Cu^{2+}-induced A $\beta_{1\text{-}42}$ aggregation: 79.7% inhibition at 25 μ M